J. Automation & Systems Engineering 9-1 (2015): 66-78

Regular paper

A New Approach Rotor Speed Estimation for PMSM Based on Sliding Mode Observer

O. Saadaoui, A. Khlaief, A. Chaari, M. Boussak, Senior Member, IEEE

JASE
Journal of Automation & Systems Engineering

Abstract-This paper proposes a sensorless speed control strategy for a permanent-magnet synchronous motor (PMSM) based on a sliding-mode observer (SMO). In order to apply a sensorless PMSM control which is robust against parameter fluctuations and disturbances, a high-speed SMO is proposed, which estimates the rotor position and the angular velocity. The stability of the proposed SMO was verified using the Lyapunov method to determine the observer gain. At standstill, the type of sliding mode observer is not able to detect the rotor position. For this reason, we use the method of voltage pulses to detect it. The simulation results show the effectiveness of the observer with sliding mode. They are characterized by a very small estimation error for the various rotational speeds (high speed, low speed).

Keywords: Permanent magnet synchronous motor (PMSM), sensorless, sliding mode observer (SMO), vector control, initial rotor position estimation.

1. INTRODUCTION

The permanent magnet synchronous motors attract the industrial world attention thanks to their superior advantages, for instance their higher efficiency, low inertia, high torque to current ratio. As an important application of PMSM, the motion control requires not only the accurate knowledge of rotor position for field orientation but also the information of rotor speed for closed-loop control; thus, position transducers such as an optical encoder and a resolver are needed to be installed on the shaft [1], [2]. However, these sensors are expensive and very sensitive to environmental constraints such as vibration and temperature [2]. To overcome these problems, instead of using position sensors, a sensorless control method has been developed for control of the motor [3], [5].

Currently, the sensorless control technology can mainly be classified into two types: the estimation method based on observer [6], [7] and the high-frequency injection method using the salient effect of motor [8]. We choose the first method seen that it is widely used because of its simple algorithm and robustness, which makes up for the dependence of the observer on the model to a certain extent [9]. Based on the technique of sliding modes, two nonlinear observers have been presented: The first used it partly a common technique in the literature is based on the estimation of electromotive force (EMF) since they are proportional to the mechanical parameters [10], [11], and the second is based on the full model [12].

O. Saadaoui, A. Khlaief and A. Chaari are with the Unit of Research C3S, ENSIT – University of Tunis – Tunisia. (e-mail:saadaoui.oussama1@gmail.com, khlaief.omar@yahoo.fr,assil.chaari@esstt.rnu.tn).
M. Boussak is with Laboratoire des Sciences de l'Information et des Systemes (LSIS) – UMR CNRS 7296 – Ecole Centrale Marseille (ECM) – 38 rue Frederic-Joliot Curie –13451 Marseille Cedex 20 – France, (e-mail: mohamed.boussak@centrale-marseille.fr).

Copyright © JASE 2015 on-line: jase.esrgroups.org

At start-up to the method of sensorless control of PMSM we find problems. The detection of initial position classified at the head of these problems, because the nonlinear observers are not able to do this detection. In [14] the authors estimate the initial rotor position in function of the inductance while using the stator currents and phase voltages. Another technique for estimation of the initial rotor position is based on tests of voltage pulse [15], [16].

In this paper, we present a sensorless speed and position vector control for a PMSM based on the SMO. This paper is organized as follows. In section 2, the mathematical model of PMSM is given. The observer design is detailed in section 3. Then, the technique of the initial rotor position is explained in section 4. A numerical application will be treated to validate the theoretical concepts is presented in section 5.

2. MATIMATICAL MODEL OF PMSM

The PMSM model in the stationary reference frame (α, β) is shown as follows:

$$\begin{cases} \dfrac{di_\alpha}{dt} = -\dfrac{R_s}{L_s} i_\alpha + \dfrac{N_p K_e}{L_s}\Omega\sin(\theta) + \dfrac{1}{L_s}V_\alpha \\ \dfrac{di_\beta}{dt} = -\dfrac{R_s}{L_s} i_\beta + \dfrac{N_p K_e}{L_s}\Omega\cos(\theta) + \dfrac{1}{L_s}V_\beta \\ \dfrac{d\Omega}{dt} = \dfrac{N_p K_e}{J}\left(i_\beta\cos(\theta) - i_\alpha\sin(\theta)\right) - \dfrac{f}{J}\Omega \\ \dfrac{d\theta}{dt} = \Omega \end{cases} \tag{1}$$

where i_α, i_β and V_α, V_β are the phase currents, and phase voltages, respectively, R_s is the stator phase resistance, L_s is the stator phase inductance, K_e is the flux created by the rotor magnets, Ω is the rotor mechanical speed, and θ is the rotor angular position.

3. OBSERVER DESIGN

The sliding mode observer is based on a stator current estimator as the stator currents and voltages are the only measured states in a PMSM drive system. Then a sliding mode observer can be designed as follows

$$\begin{cases} \dfrac{d\hat{i}_\alpha}{dt} = -\dfrac{R_s}{L_s}\hat{i}_\alpha + \dfrac{N_p K_e}{L_s}\hat{\Omega}\sin(\hat{\theta}) + \dfrac{1}{L_s}V_\alpha + K_1\,\mathrm{sgn}(\bar{i}_\alpha) \\ \dfrac{d\hat{i}_\beta}{dt} = -\dfrac{R_s}{L_s}\hat{i}_\beta + \dfrac{N_p K_e}{L_s}\hat{\Omega}\cos(\hat{\theta}) + \dfrac{1}{L_s}V_\beta + K_1\,\mathrm{sgn}(\bar{i}_\beta) \\ \dfrac{d\hat{\Omega}}{dt} = \dfrac{N_p K_e}{J}\left(\hat{i}_\beta\cos(\hat{\theta}) - \hat{i}_\alpha\sin(\hat{\theta})\right) - \dfrac{f}{J}\hat{\Omega} + K_2\,\mathrm{sgn}(\bar{i}_\alpha) + K_2\,\mathrm{sgn}(\bar{i}_\beta) \\ \dfrac{d\hat{\theta}}{dt} = \hat{\Omega} + K_3\,\mathrm{sgn}(\bar{i}_\alpha) + K_3\,\mathrm{sgn}(\bar{i}_\beta) \end{cases} \tag{2}$$

with $\bar{i}_\alpha = i_\alpha - \hat{i}_\alpha$, $\bar{i}_\beta = i_\beta - \hat{i}_\beta$ and K_1, K_2 and K_3 are the observer gains.
The equations of dynamic errors are :

$$\begin{cases} \dot{\bar{i}}_\alpha = -\dfrac{R_s}{L_s}\bar{i}_\alpha + \dfrac{N_p K_e}{L_s}\left(\Omega\sin\theta - \hat{\Omega}\sin\hat{\theta}\right) - K_1\,\mathrm{sgn}\left(\bar{i}_\alpha\right) \\ \dot{\bar{i}}_\beta = -\dfrac{R_s}{L_s}\bar{i}_\beta + \dfrac{N_p K_e}{L_s}\left(-\Omega\cos\theta + \hat{\Omega}\cos\hat{\theta}\right) - K_1\,\mathrm{sgn}\left(\bar{i}_\beta\right) \\ \dot{\bar{\Omega}} = \dfrac{N_p K_e}{J}\left(i_\beta\cos\theta - i_\alpha\sin\theta\right) - \left(\hat{i}_\beta\cos\hat{\theta} - \hat{i}_\alpha\sin\hat{\theta}\right) - \dfrac{f}{J}\bar{\Omega} - K_2\,\mathrm{sgn}\left(\bar{i}_\alpha\right) - K_2\,\mathrm{sgn}\left(\bar{i}_\beta\right) \\ \dot{\bar{\theta}} = \Omega - \hat{\Omega} - K_3\,\mathrm{sgn}\left(\bar{i}_\alpha\right) - K_3\,\mathrm{sgn}\left(\bar{i}_\beta\right) \end{cases} \tag{3}$$

with $\bar{\Omega} = \Omega - \hat{\Omega}$ and $\bar{\theta} = \theta - \hat{\theta}$

This analysis allowed us to know the interval of gains associated with the observer for which the system is designed stable.

The analysis of the observer convergence will be carried out using the following Lyapunov function:

$$V = \frac{1}{2}\left(\bar{i}_\alpha^{\,2} + \bar{i}_\beta^{\,2} + \bar{\Omega}^2 + \bar{\theta}^2\right) \tag{4}$$

Its derivative is

$$\dot{V} = \bar{i}_\alpha\dot{\bar{i}}_\alpha + \bar{i}_\beta\dot{\bar{i}}_\beta + \bar{\Omega}\dot{\bar{\Omega}} + \bar{\theta}\dot{\bar{\theta}} \tag{5}$$

It yields

(6)

with $a_1 = \dfrac{R_S}{L_S}$, $a_2 = \dfrac{N_p K_e}{L_S}$, $a_2 = \dfrac{N_p K_e}{J}$, $a_4 = \dfrac{f}{J}$

$$\begin{aligned} \left|\bar{i}_\alpha\right| &= i_\alpha\,\mathrm{sgn}\left(\bar{i}_\alpha\right) \\ \left|\bar{i}_\beta\right| &= i_\beta\,\mathrm{sgn}\left(\bar{i}_\beta\right) \end{aligned} \tag{7}$$

To guarantee the convergence, the time derivative of the candidate Lyapunov function is forced such that $\dot{V} < 0$.

Knowing that

$$\begin{aligned} &-a_1\bar{i}_\alpha^{\,2} < 0,\ -a_1\bar{i}_\beta^{\,2} < 0,\ -a_4\bar{\Omega}^2 < 0 \\ &\left|\Omega\sin\theta - \hat{\Omega}\sin\hat{\theta}\right| < 2\Omega_{\max} \\ &\left|\bar{i}_\alpha(\Omega\sin\theta - \hat{\Omega}\sin\hat{\theta})\right| < 4i_{\max}\Omega_{\max} \end{aligned} \tag{8}$$

It is sufficient to choose K_1, K_2 and K_3 such that

$$\begin{aligned} &a_2\bar{i}_\alpha\left(\Omega\sin\theta - \hat{\Omega}\sin\hat{\theta}\right) - K_1\left|\bar{i}_\alpha\right| + a_2\bar{i}_\beta\left(\Omega\cos\theta - \hat{\Omega}\cos\hat{\theta}\right) \\ &-K_1\left|\bar{i}_\beta\right| + a_3\bar{\Omega}\left[(i_\beta\cos\theta - i_\alpha\sin\hat{\theta}) - (\hat{i}_\beta\cos\hat{\theta} - \hat{i}_\alpha\sin\hat{\theta})\right] \\ &-\bar{\Omega}K_2\mathrm{sgn}(\bar{i}_\alpha) - \bar{\Omega}K_2\mathrm{sgn}(\bar{i}_\beta) + \bar{\theta}\ \bar{\Omega} - \bar{\theta}K_3\mathrm{sgn}(\bar{i}_\alpha) - \bar{\theta}K_3\mathrm{sgn}(\bar{i}_\beta) < 0 \end{aligned} \tag{9}$$

thus, the gains will be tuned such as

$$K_1 > 2a_2\Omega_{\max},\ K_2 > 2a_3 i_{\max} \text{ and } K_3 > \Omega_{\max} \tag{10}$$

Based on analysis of the aspects mentioned above, Fig.1 shows the block diagram of the sensorless control of PMSM using the sliding mode observer. We take $u_{\alpha,\beta}$ and $i_{\alpha,\beta}$ as input of the SMO, these parameters can eliminate the effect of dead time of the inverter.

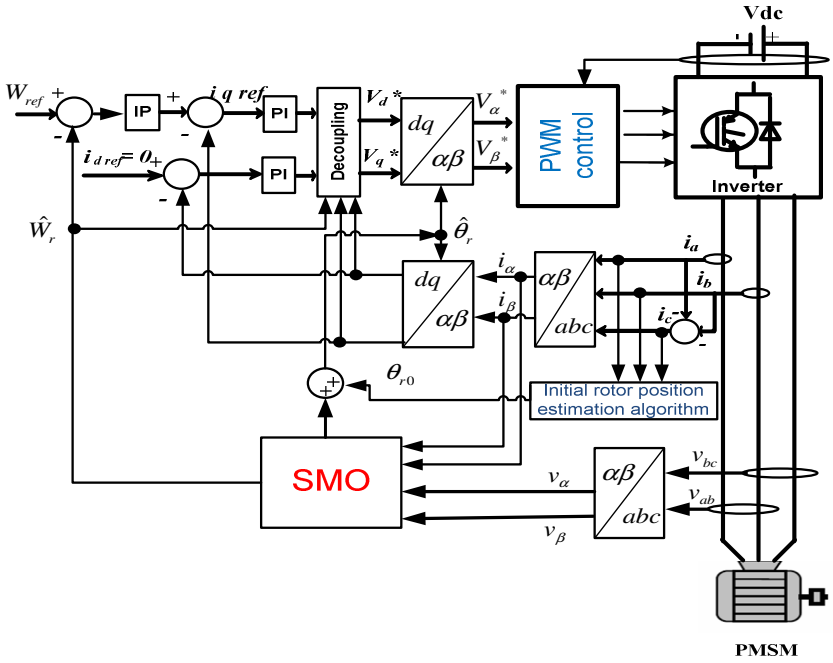

Figure 1 Block diagram of sensorless vector control of PMSM

4. INITIAL ROTOR POSITION ESTIMATION

In this part, we are interested in the voltage pulses method published in [13].

4.1 The Proposed Detection Method

At standstill, the expression of the current of the phase a is given by:

$$\frac{d}{dt}(I_a)=\frac{4}{9}\left(\frac{L_0+L_1\cos(2\theta_{r0})}{{L_0}^2-{L_1}^2}\right)v_{ab}=\frac{4}{9}\left(\frac{L_0+L_1\cos(2\theta_{r0})}{{L_0}^2-{L_1}^2}\right)v_{ac} \tag{11}$$

We find that the coefficient related voltages represent an admittance form

$$Y_{eq}=Y_0+Y_1\cos(2\theta_{r0}) \tag{12}$$

with $Y_0=\frac{4}{9}\left(\frac{L_0}{{L_0}^2-{L_1}^2}\right)$ and $Y_1=\frac{4}{9}\left(\frac{L_2}{{L_0}^2-{L_1}^2}\right)$.

Applying a positive voltage pulse $U_1(C_1\bar{C}_2\bar{C}_3)$ at the terminals of the phase motor generates a current in the form

$$I_a=I_0+\Delta I_a=I_0+\Delta I_0\cos(2\theta_{r0}) \tag{13}$$

with $I_0=\frac{1}{3}(I_a+I_b+I_c)$ is the dc current component.

In the same manner, the expressions of the currents which correspond to the voltage vector $U_2(\bar{C}_1C_2\bar{C}_3)$ and $U_3(\bar{C}_1\bar{C}_2C_3)$ are expressed by

$$\begin{cases} I_b = I_0 + \Delta I_0 \cos(2\theta_{r0} - \frac{2\pi}{3}) \\ I_c = I_0 + \Delta I_0 \cos(2\theta_{r0} + \frac{2\pi}{3}) \end{cases} \quad (14)$$

We can notice that the monotonous function lets us to replace the stator currents by their respective difference ΔI_a , ΔI_b and ΔI_c . The expression of the rotor position estimation can be written as:

$$\theta_{r0} = \frac{\sqrt{3}}{2} \frac{(\Delta I_a - \Delta I_b)}{(2\Delta I_a - \Delta I_b - \Delta I_c)} \text{ or } \theta_{r0} = \frac{\sqrt{3}}{2} \frac{(\Delta I_a - \Delta I_b)}{(2\Delta I_a - \Delta I_b - \Delta I_c)} + 180° \quad (15)$$

While using (15), we can establish the Table II permitting to detect the initial rotor position.

TABLE I. TABLE OF INITIAL POSITION ESTIMATION

θ_{r0}	Sign of the Differences	Sign of the peaks	Sign of the peaks
15°-30° or 195°-210°	$\Delta I_a - \Delta I_c > 0$	$\Delta I_b < 0$	$\Delta I_a > 0$
30°-45° or 210°-225°	$\Delta I_c - \Delta I_a > 0$	$\Delta I_b < 0$	$\Delta I_a > 0$
45°-60° or 225°-240°	$\Delta I_a - \Delta I_b > 0$	$\Delta I_c > 0$	$\Delta I_a < 0$
60°-75° or 240°-255°	$\Delta I_b - \Delta I_a > 0$	$\Delta I_c > 0$	$\Delta I_a < 0$
75°-90° or 255°-270°	$\Delta I_c - \Delta I_b > 0$	$\Delta I_a < 0$	$\Delta I_b > 0$
90°-105° or 270°-285°	$\Delta I_b - \Delta I_c > 0$	$\Delta I_a < 0$	$\Delta I_b > 0$
105°-120° or 285°-300°	$\Delta I_c - \Delta I_a > 0$	$\Delta I_b > 0$	$\Delta I_a < 0$
120°-135° or 300°-315°	$\Delta I_a - \Delta I_c > 0$	$\Delta I_b > 0$	$\Delta I_a < 0$
135°-150° or 315°-330°	$\Delta I_b - \Delta I_a > 0$	$\Delta I_c < 0$	$\Delta I_a > 0$
150°-165° or 330°-345°	$\Delta I_a - \Delta I_b > 0$	$\Delta I_c < 0$	$\Delta I_a > 0$
165°-180 or 345°-360°	$\Delta I_b - \Delta I_c > 0$	$\Delta I_a > 0$	$\Delta I_b < 0$
180°-195° or 360°-375°	$\Delta I_c - \Delta I_b > 0$	$\Delta I_a > 0$	$\Delta I_b < 0$

According to the Table I we can note that it is possible to detect the initial rotor position with two different values. This problem is resolved in section IV.B.

4.2 Discrimination of the Uncertainty of the Initial Rotor Position

This method consists in apply a pulse voltage to saturate the machine. For it, we will argue in the following figure.

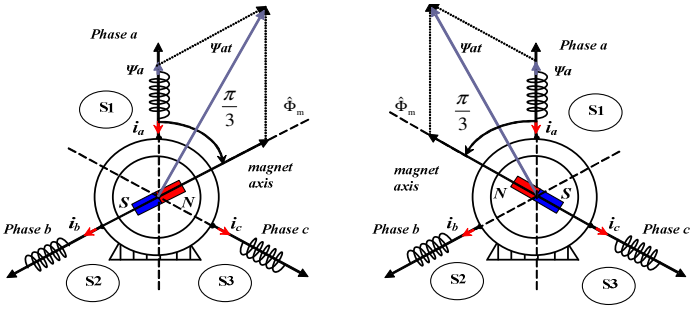

Figure 2 Discrimination of the two values of the initial rotor position

Fig. 2. shows the discrimination of the two values of the initial rotor position. If the magnet flux is in the same direction to the one generated by the current pulse, we get an additive flux and therefore a large peak current. In the opposite case, we obtain a decreasing field. Consequently the initial rotor position corresponds to a current of the most important variation. When the north pole of the magnet field is near to the one axis of the three phase's windings, the current peak is most important in the considered phase. By making a synthesis of the study previously developed to avoid the ambiguity on the accuracy concerning the rotor initial position estimation we can make the Table II:

TABLE II. DISCRIMINATION OF THE UNCERTAINTY OF THE INITIAL ROTOR POSITION

Voltage pulse	Peak value of the current	Location of the initial position
$U_1\left(C_1\bar{C}_2\bar{C}_3\right)$	$I_a > I_b,\ I_a > I_c$	$-60° < \theta_{r0} < 60°$
$U_2\left(\bar{C}_1C_2\bar{C}_3\right)$	$I_b > I_a,\ I_b > I_c$	$60° < \theta_{r0} < 180°$
$U_3\left(\bar{C}_1\bar{C}_2C_3\right)$	$I_c > I_b,\ I_c > I_a$	$180° < \theta_{r0} < 360°$

5. INITIAL ROTOR POSITION ESTIMATION

In order to verify the validity of the SMO, the proposed system from Fig. 1 has been implemented in the Matlab/Simulink programming environment. The parameters of the tested PMSM are given in Table III.

We simulated 2 experimental cases: case 1 and case 2. In case 1, we started the motor with zero initial position (in this case $\theta_{r0} = 0$).

Fig. 3 shows the simulation results of high-speed sensorless control using the sign function, fig. 3 (a) shows the actual speed follows the estimated value for a cycle speed of 300 rad/s and -300 rad/s, Fig.3 (b) shows the appearance of the actual and estimated position during the reversal of the direction of rotation, Fig.3 (c) gives the appearance of the electrical error speed, Fig.3 (d) shows the change of the electrical error position during the operating cycle. From this figure, we noted that the estimated position coincides with that measured in the cycle.

Fig. 4 shows the simulation results of low-speed sensorless control using the sign function for a speed cycle of 8 rad/s at 20 rad/s. In case 2, we changed the value initial position to $\theta_{r0} = \frac{\pi}{4}$.

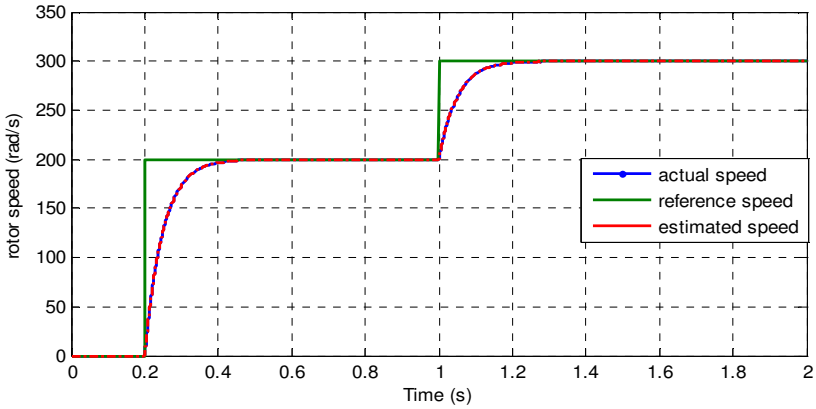
rotor speed (rad/s)
Time (s)
actual speed
reference speed
estimated speed

(a)

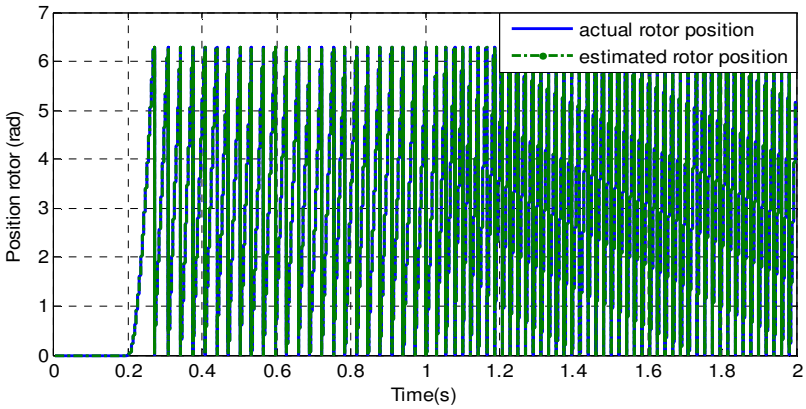
Position rotor (rad)
Time(s)
actual rotor position
estimated rotor position

(b)

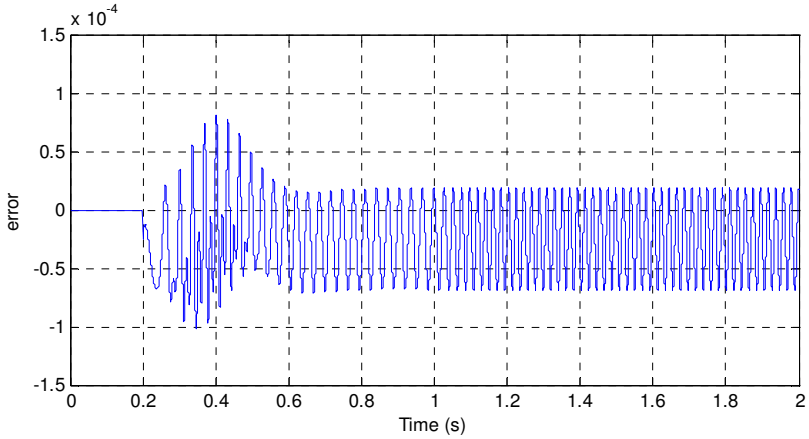
x 10^-4
error
Time (s)

(c)

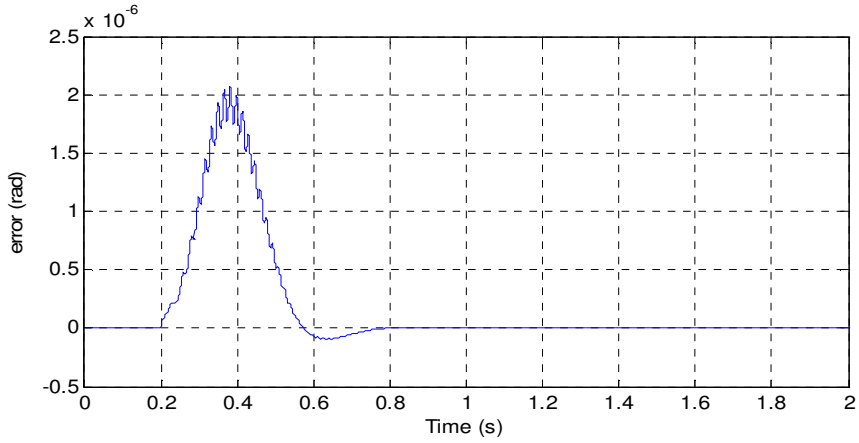

(d)

Figure 3 Sensorless high-speed control using the sign function. (a) Actual and estimated speeds. (b) Actual and estimated rotor position. (c) Electrical error speed. (d) Electrical error position (case 1).

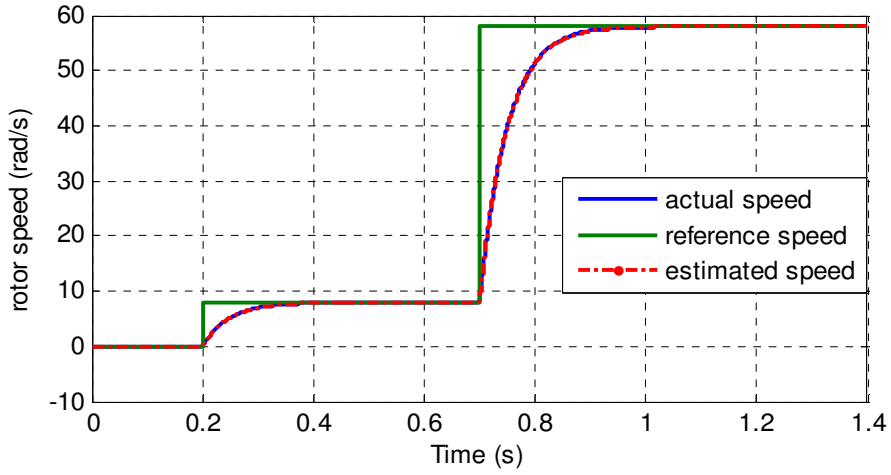

(a)

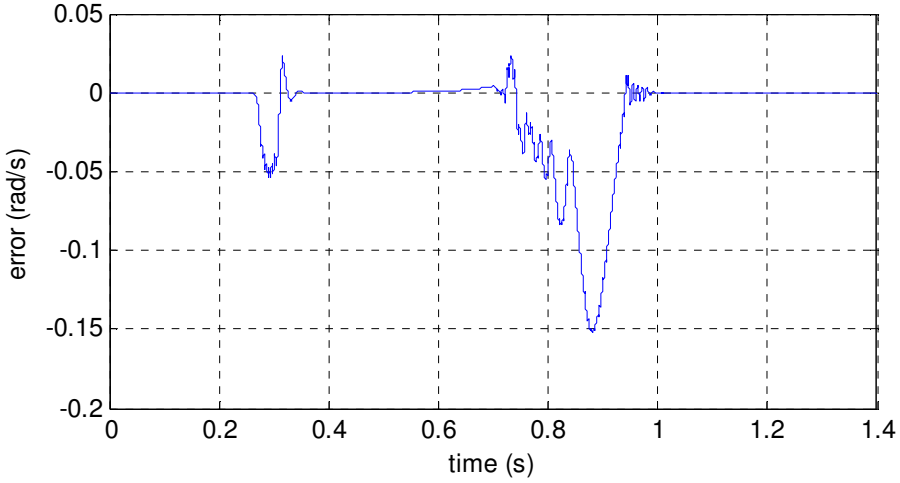

(b)

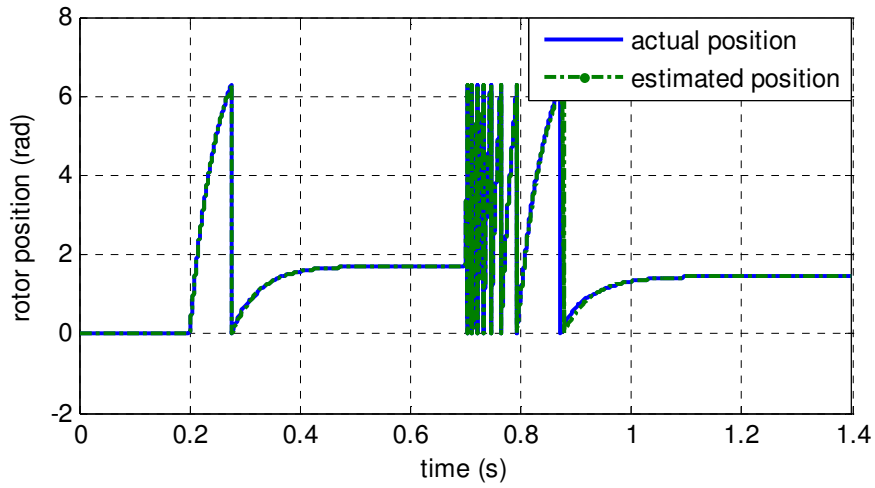

(c)

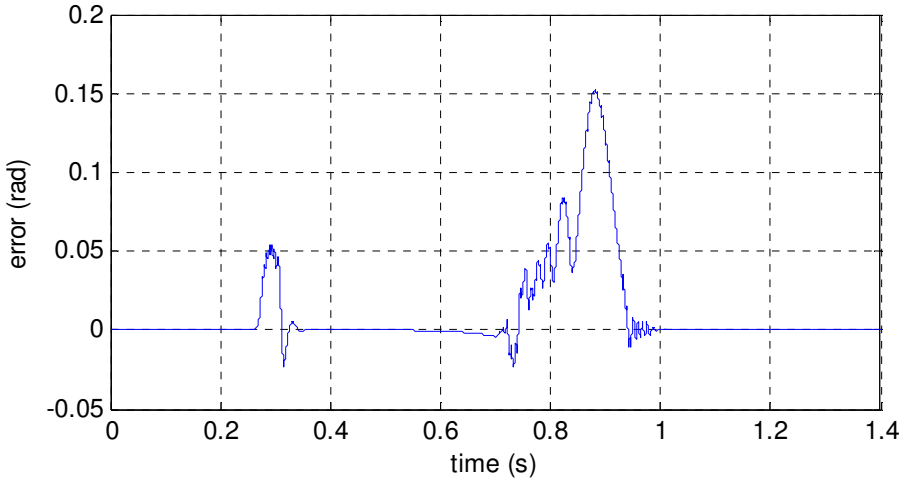

(d)

Figure 4 Sensorless low-speed control using the sign function. (a) Actual and estimated speeds. (b) Actual and estimated rotor position. (c) Electrical error speed. (d) Electrical error position (case 1).

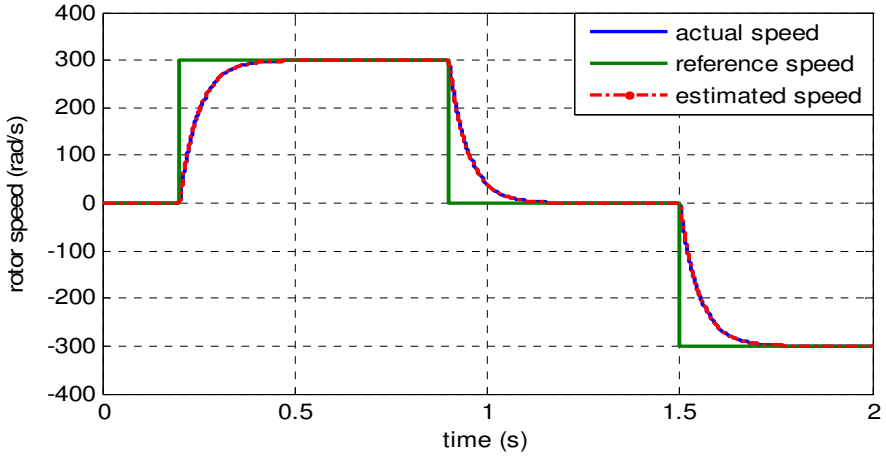

(a)

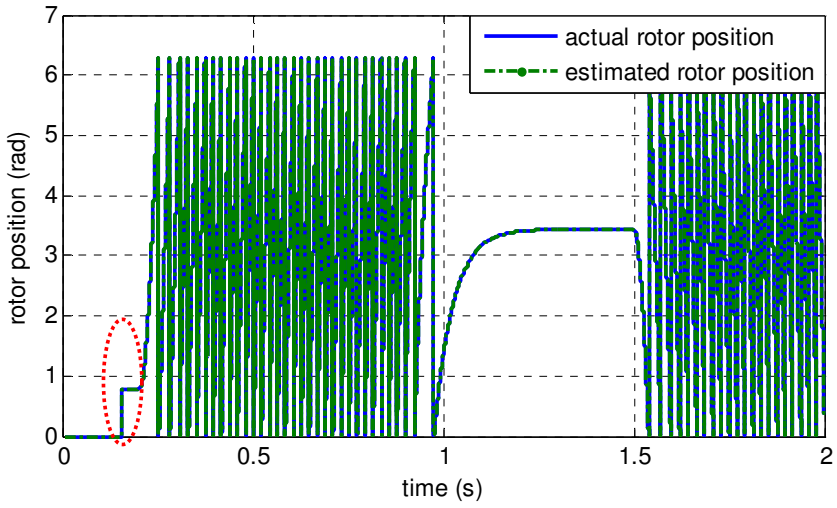

(b)

Figure 5 Sensorless high-speed control using the sign function. (a) Actual and estimated speeds. (b) Actual and estimated rotor position (case 2).

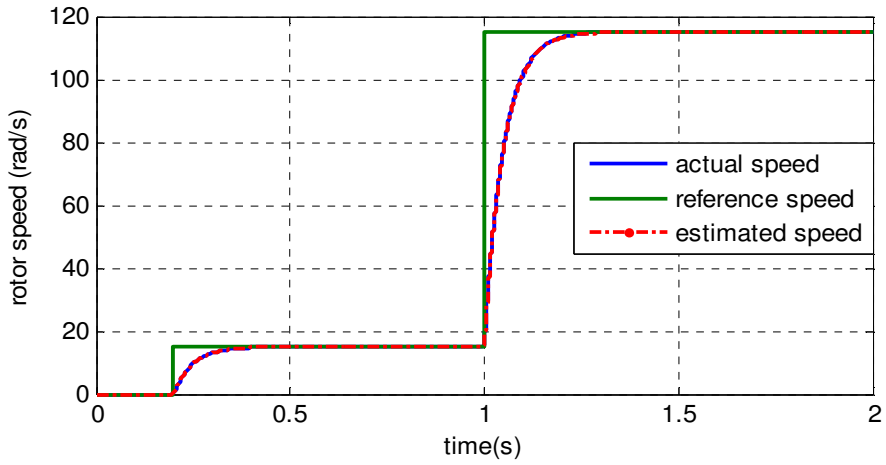

(a)

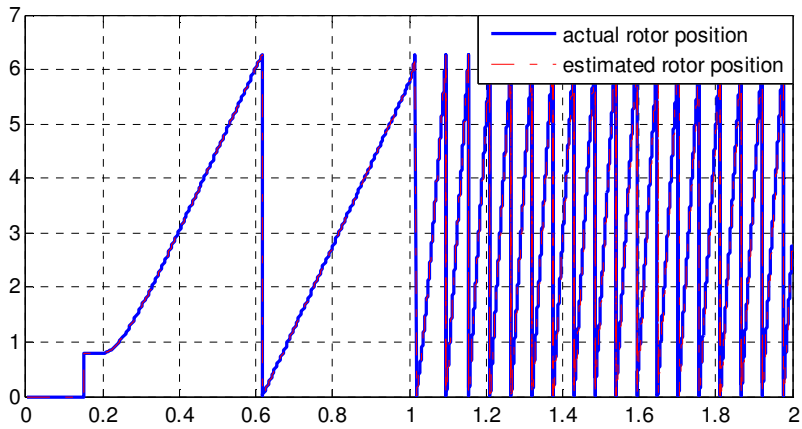

(b)

Figure 6 Sensorless low-speed control using the sign function. (a) Actual and estimated speeds. (b) Actual and estimated rotor position (case 2).

Fig. 5 and 6 show the all estimated magnitudes using the SMO for the various rotational speeds. In fig. 5(a) and 6(a), we note that the response of the estimated speed is similar to that measured following reference speed. Fig. 5(b) and 6(b) show the appearance of actual and estimated position during the start-up and the direction reversal of the rotation.
We also note that the simulation results show the validity of the method applied for estimation of the initial rotor position of the PMSM.

6. CONCLUSIONS

A sensorless robust control of a permanent magnet synchronous motor has been presented. The sensorless scheme is achieved via a sliding mode observer that estimates the speed and the position of a PMSM. The stability of the SMO has been proved with the use of a Lyapunov stability analysis. In this paper, we apply a technique to detect the initial rotor position based on tests of voltage pulses applied to the machine at standstill state.
Simulation results validate the feasibility and effectiveness of the SMO for estimating the rotor position and speed of the PMSM. Therefore, future work will focus on experimental validation using test bench based on the DS1103 card from dSpace to verify the proposed method.

APPENDIX

TABLE III . PARAMETERS OF THE MOTOR

Parameters	Values	units
Stator resistor R_s	6.2	Ω
Stator inductance L_s	32.8962	mH
Pole pairs N_p	3	--
Flux of permanent magnet Φ_f	0.305	Wb
Rotational inertia J	0.0036	Nm/A
Rated speed Ω_n	3000	tr/min
Torque constant K_t	0.9149	Nm/A
DC voltage U_{dc}	540	540
Rated torque C_n	4	A
Friction coefficient *f*	0.0011	Nm/rd/s

The PI controllers of d and q-axis current are made up by the following parameters:
$K_{p\_i_d} = 2200$, $K_{i\_i_d} = 40$, $K_{p\_i_q} = 400$ and $K_{i\_i_q} = 40$.
The parameters of IP speed controller are: $K_{p\_\Omega} = 15$ and $K_{i\_\Omega} = 20$.
Observer gain $K1 = 10000$, $K2 = 6000$ and $K3 = 10$, $K4 = 5$.

REFERENCES

[1] H. Liu, and S. Li, "Speed Control for PMSM Servo System Using Predictive Functional Control and Extended State Observer," IEEE Trans. Ind. Electron, Vol. 59, No. 2, February 2012, pp. 1171-1183.

[2] B. Alesca, M. N. Cirstea, and A. Onea, "Simulink Modeling and Design of an Efficient Hardware-constrained FPGA-based PMSM Speed Controller," IEEE Trans. Ind. Informat, Vol. 8, No. 3, August 2012, pp. 554-562.

[3] R. Wu, and G. R. Selmon, "A Permanent Magnet Motor Drive Without a Shaft Sensor," IEEE Trans. Ind. Appl., Vol. 27, No. 5, Sep./Oct. 1991, pp. 1005-1011.

[4] F. Parasiliti, R, Petrella and M. Tursini, "Sensorless Speed Control of a PM Synchronous Motor by Sliding Mode Observer," In Proc. IEEE ISIE, Vol. 3, Jul. 1997, pp. 1106-1111.

[5] S. Chi, Z, Zhang, and L. Xu, "Sliding-mode Sensorless Control of Directdrive PM Synchronous Motors for Washing Machine Applications," IEEE Trans. Ind. Appl., Vol. 45, No. 2, Mar. 2009, pp. 582-590.

[6] P. Tomei, and C. M. Verrelli, "Observer-based Speed Tracking Control for Sensorless Permanent Magnet Synchronous Motors with Unknown Load Torque," IEEE Trans. Autom. Control, Vol. 56, No. 6, Jun. 2011, pp. 1484-1477.

[7] A. Khlaief, M. Boussak, and M. Gossa, "Sensorless Speed Vector Control of PMSM Drive Based on MRAS Method," 11 th International Conference on Sciences and Techniques of Automatic Control & Computer Engineering STA 2010, CDROM.

[8] Z. Q. Zhu, and L. M. Gong, "Investigation of Effectiveness of Sensorless Operation in Carrier-Signal-Injection-Based Sensorless-Control Methods," IEEE Trans. Ind. Electron., Vol. 58, No. 8, Aug. 2011, pp. 3431-3439.

[9] J. B. Chu, Y. W. Hu, W. X. Huang, M. J. Wang, J.F Yang, and Y. X. Shi, "An Improved Sliding Mode Observer for Position Sensorless Vector Control Drive of PMSM," In Proc. IEEE Power Electron. Motion Control Conf., May 2009, pp. 1898-1902.

[10] M. Ezzat, A. Glumineau, and F. Plestan, "Sensorless High Order Sliding Mode Control of Permanent Magnet Synchronous Motor," International Workshop on Variable Structure Systems, Mexico, 2010.

[11] Z. Qiao, T. Shi, Y. Wang, Y. Yan, C. Xia, and X. He, "New Sliding Mode Observer for Position Sensorless Control of Permanent Magnet Synchronous Motor," IEEE Trans. Ind. Electron., Vol. 60, 2013, pp. 710-719.

[12] M. Ezzat, A. Glumineau et R. Boisliveau, "Comparaison de deux observateurs non linéaires pour la commande sans capteur de la MSAP : validation expérimentale," CIFA. 2010, pp. 6.

[13] M. Boussak, "Implementation and Experimental Investigation of Sensorless Speed Control With Initial Rotor Position Estimation for Interior Permanent Magnet Synchronous Motor Drive," IEEE Trans. Power Electron., Vol. 20, No. 6, Nov. 2005, pp. 1413-1421.

[14] M. E. Haque, L. Zhong, M. F. Rahman, "A Sensorless Initial Rotor Position Estimation Scheme for a Direct Torque Controlled Interior Permanent Magnet

Synchronous Motor Drive," IEEE Trans. Power Electron., Vol. 18, No. 6, Nov. 2003, pp. 1376-1383.

[15] M. Tursini, R. Petrella, and F. Parasiliti, "Initial Rotor Position Estimation Method for PM Motors," IEEE Trans. Power Electron., Vol. 39, No. 6, Nov./Dec. 2003, pp. 1630-1640.

[16] A. Khlaief, M. Bendjedia, and M. Boussak, "A Nonlinear Observer for High-Performance Sensorless Speed Control of IPMSM Drive," IEEE Trans. Power Electron., Vol. 27, No. 6, June 2012, pp. 3028-3040.